A General Atmospheric Pressure Chemical Vapor Deposition Synthesis and Crystallographic Study of Transition-Metal Sulfide One-Dimensional Nanostructures

Jian-Ping Ge,[a] Jin Wang,[a] Hao-Xu Zhang,[a, b] and Ya-Dong Li*[a]

Abstract: A series of transition-metal sulfide one-dimensional (1D) nanostructures have been synthesized by means of a general atmospheric pressure, chemical vapor deposition (APCVD) strategy. Vapour–liquid–solid (VLS) and vapour–solid (VS) mechanisms, along with the results of SEM and TEM observations, were used to explain the formation of these nanostructures. The regularity of the growth in the direction of the hexagonal nanowire is explored; we find that it prefers to grow along (100), (110), or (00x) directions owing to particular crystal structures. The adopted synthetic route was expected to provide abundant useful 1D building blocks for the research of mesoscopic physics and fabrication of nanoscale devices.

Keywords: chemical vapor deposition · nanostructures · sulfur · transition metals

Introduction

During the past decades, transition-metal sulfides have attracted great interest due to their physical and chemical properties. For instance, CdS[1–2] is widely used for photoelectric conversion in solar cells and in light-emitting diodes for flat-panel displays; ZnS[3–4] is a famous luminescence material with various luminescence properties; CoS and MnS[5–6] are applied in the fabrication of diluted magnetic semiconductors; and NiS[7–9] is used as a metal insulator, in magnetic phase transformation, and in hydrogenation catalysis.

Recently, one-dimensional (1D) nanostructures, such as wires, rods, belts, and tubes have become the focus of intensive research owing to their unique applications in mesoscopic physics and fabrication of nanoscale devices.[10–13] It is generally accepted that 1D nanostructures provide a good system to investigate the dependence of electrical and thermal transport or mechanical properties on dimensionality and size confinement. Therefore, the ability to generate such 1D nanostructures is essential to much of modern science and technology.

As to transition-metal sulfides, various strategies have been applied to fabricate their 1D nanostructures. Directed by a template, a single-crystal CdS[14] nanowire array could be synthesized on a porous alumina, and WS_2[15] nanotubes could be prepared from the pyrolysis of artificial lamellar mesostructures formed by a soft organic surfactant. The solvothermal method[16–18] has been extensively exploited to produce a variety of sulfide nanowires, rods, and tubes. In the aspect of gas-phase synthesis, a laser-assisted catalytic growth (LCG) method[18–20] was reported to produce many semiconductor nanowires. Illumined and stimulated by the synthesis of oxide nanobelts,[21] thermal evaporation methods have also been developed to grow ZnS nanoribbons[22] and CdS nanowires[23] on a large scale. Otherwise, Cu_2S[24] nanowires were transformed by sulfuration of the oxide intermediate. Here, as a typical example, we will first report an atmospheric pressure chemical vapor deposition (APCVD) process to prepare heterostructural NiS/SiO_2 nanowire/nanotubes (NW/NTs) on a Si substrate. Then, a novel one-step route was developed to fabricate a series of transition-metal sulfide 1D nanostructures on an Si substrate; this might provide abundant resources to the research of mesoscopic physics and fabrication of nanoscale devices.

[a] J.-P. Ge, J. Wang, Dr. H.-X. Zhang, Prof. Y.-D. Li
The Key Laboratory of Atomic and Molecular Nanoscience
Ministry of Education, Department of Chemistry
Tsinghua University, Beijing 100084 (China)
Fax: (+86) 10-62788765
E-mail: ydli@mail.tsinghua.edu.cn

[b] Dr. H.-X. Zhang
Nanoscale Physics & Devices Laboratory
Institute of Physics, Chinese Academy of Science
Beijing 100080 (China)

Supporting information for this article is available on the WWW under http://www.chemeurj.org/ or from the author.

 DOI: 10.1002/chem.200400008

Results and Discussion

APCVD and characterization of NiS/SiO_2 nanowire/nanotubes: Figure 1 displays a series of typical scanning electron microscope (SEM) images of the as-prepared NiS/SiO_2 NW/NTs deposited on a (100) Si substrate. The SEM images

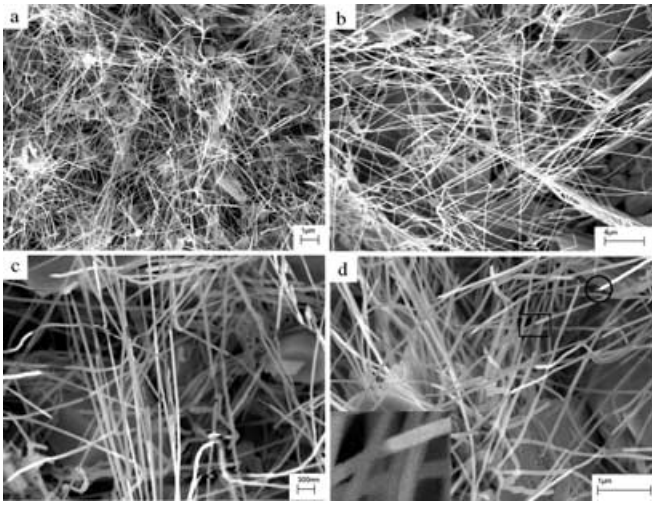

Figure 1. SEM image of the as-prepared NiS/SiO_2 NW/NTs. a) and b) Overall images of the NiS/SiO_2 NW/NTs. c) and d) Relative high-resolution SEM images of the NiS/SiO_2 NW/NTs. The inset clearly shows the hetero-junction structure. The bars represent 1 μm, 4 μm, 300 nm, and 1 μ in a)–d), respectively.

shows that the substrate was covered with pure NiS/SiO_2 NW/NTs with an average diameter of 50 nm and length of 10 μm. High-resolution SEM image shows an evident junction between NiS NWs and SiO_2 NTs (Figure 1d, inset).

In addition, transmission electron microscope (TEM) images of individual NW/NTs provide further insight into the structure of these materials. Results from energy-dispersive X-ray spectroscopy (EDS) characterization show that the nanowires primarily contain Ni and S. (Figure 2a inset; the Si peak in the figure was caused by SiO_2 covering the outside the NiS nanowire). Nanotubes with the same diameter are observed to grow out of one end of the nanowires, and the corresponding EDS spectrum demonstrates that the nanotubes mainly consist of Si and O atoms. The electron diffraction (ED) pattern (Figure 2b, inset) reveals the intrinsic structure of the amorphous SiO_2 nanotube. Together with the HRTEM image, it shows that the nanotube is made of amorphous SiO_2. Figure 2c shows two crystal faces present 120° angle at the junction position; this helps us to understand the crystal growth of the nanowire described later in this article. Figure 2d is the ED pattern of the nanowire, indexed to α-NiS with the hexagonal NiAs structure. The (110) direction of the ED pattern is parallel to the wire axis, showing that growth might occur along the (110) direction. A high-resolution TEM image exhibits well-resolved (100) and (110) lattice planes. (Figure 2e) The experimental lattice spacings of 0.30 ± 0.01 nm and 0.17 ± 0.01 nm are consistent with the 0.298 nm and 0.172 nm separation in bulk crystals. (JCPDS No. 77–1624) The 30° orientation between

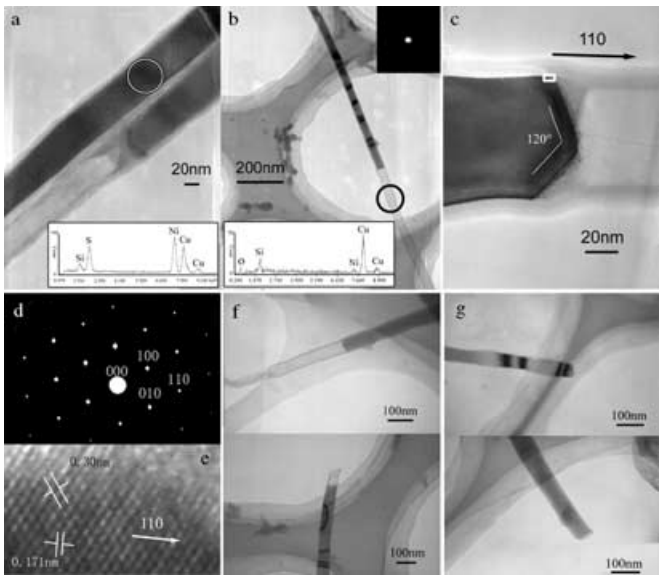

Figure 2. TEM images of the as-prepared NiS/SiO_2 NW/NTs. a) and b) TEM images of the single NiS/SiO_2 NW/NT. The inset was the corresponding EDS spectrum for the selected scanning area. c) TEM image of the hetero-junction section. d) ED patterns taken along the [001] axis. e) High-resolution TEM image of the NiS nanowire. f) Open- and closed-end tubes are both observed. g) Another end of the NiS/SiO_2 NW/NT corresponding to that shown in f).

the (100) and (110) lattice planes is also consistent with the ED patterns; this further confirm the (110) growth direction of the as-prepared nanowire.

XRD patterns, obtained by irradiating the substrate covered with NiS/SiO_2 NW/NTs without further treatment after preparation, were used to determine the chemical composition and structure of the as-prepared NW/NTs. The XRD spectrum of the product (Figure 3) could be indexed to a

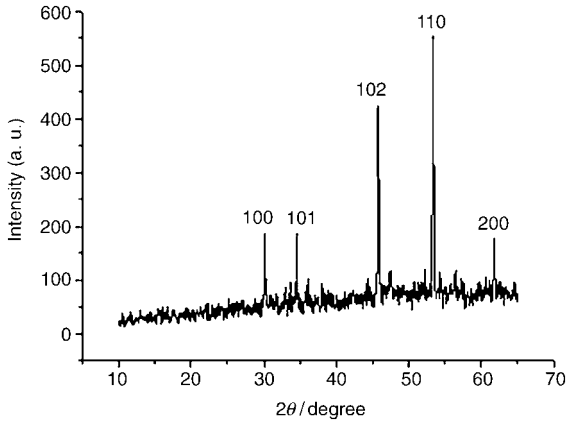

Figure 3. XRD pattern of the as-made NiS/SiO_2 NW/NTs.

pure hexagonal NiAs structure with lattice constants $a = 0.3439$ nm, $c = 0.5324$ nm (JCPDS No. 77–1624). Sharp and strong peaks also confirmed the NiS nanowires were well crystallized. No peaks due to any other phases were detected, indicating the high purity of the products. Lack of crystal SiO_2 peaks also reveals that the SiO_2 nanotube is amorphous

Figure 4 shows a schematic diagram to describe the progress of the nanocrystal growth. At first, $NiCl_2$ and S powders evaporate into vapor and are transported to the downstream end by the argon flow. Then, they combine into NiS nanostructure to generate the initial nucleation, which grows in an epitaxial way (elongated along the [1 1 0] direction) and favors the nanocrystal to form a 1D nanostructure. At the same time, evaporated Si atoms react with the trace amount of oxygen to form an amorphous SiO_2 layer outside the single-crystal NiS nanowire. During the heating process, the concentration of Ni and S atoms gradually decreases, and the growth of NiS is finally terminated. However, amorphous SiO_2 is further generated at the junction position. Catalyzed by the NiS, it grows into nanotubes with a length range from several tens of nanometers to several micrometers. Both open- and closed-end nanotubes are observed. The former are always short and the latter can grow to several micrometers.

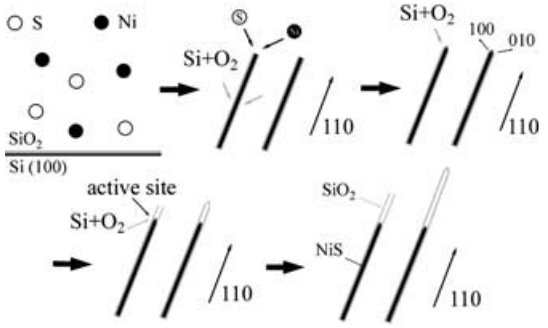

Figure 4. Mechanism for the growth of NiS/SiO_2 NW/NTs. For details see text.

APCVD to transition-metal sulfide one-dimensional nanostructures: Stimulated by the successful synthesis of NiS nanowires, we try to extend this convenient and less toxic method to the fabrication of other transitional-metal sulfide 1D nanostructures by simply replacing the chloride and controlling the specific parameter of the APCVD. Figures 5 and 6 show SEM images of the as-prepared products. The results indicate that, CdS, ZnS, CoS, NiS, MnS, and Fe_7S_8 could form wires with a large slenderness ratio, while, Cr_2S_3 and WS_2 prefer to form rods and tubes, respectively. Uniquely

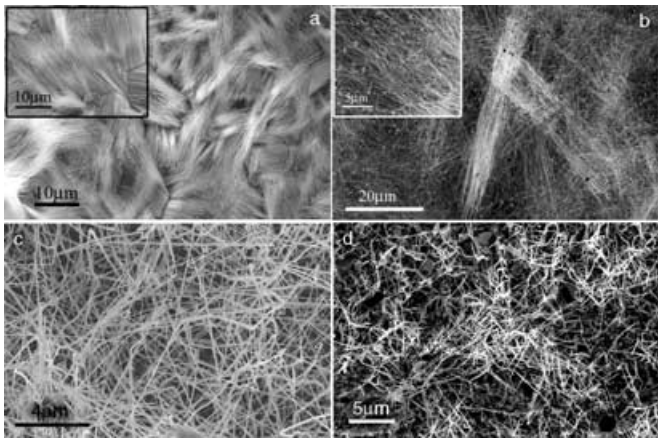

Figure 5. SEM image of the as-prepared a) CdS, b) CoS, c) MnS, and d) Fe_7S_8 nanowires. he bars represent 10, 20, 4, and 5 μ in a)–d), respectively. In the insets of a) and b), the bars represent 10 and 5 μm, respectively.

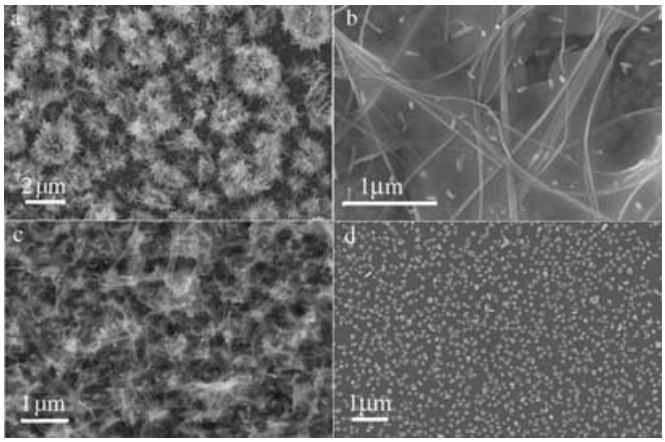

Figure 6. SEM image of the as-prepared a) Cr_2S_3 nanorod, b) WS_2 nanotube, c) ZnS nanowire, and d) $Cu_{7.2}S_4$ nanoparticle.

for Cu_xS, the main deposited products are particles (100 nm), although several long whiskers are also observed on the substrate.

XRD patterns (Figure 7) were also measured to determine the chemical composition and structure of the deposited products, and the spectra could be well indexed to the JCPDS data base. (JCPDS card CdS: No.77–2306; ZnS: No. 75–1547; $Cu_{7.2}S_4$: No.72–1966; CoS: No.75–0605; Fe_7S_8: No.76–2308; MnS: No.72–1534; Cr_2S_3: No.72–1223; WS_2: No.84–1398) The specific descriptions of the structure and morphology are summarized in Table 1.

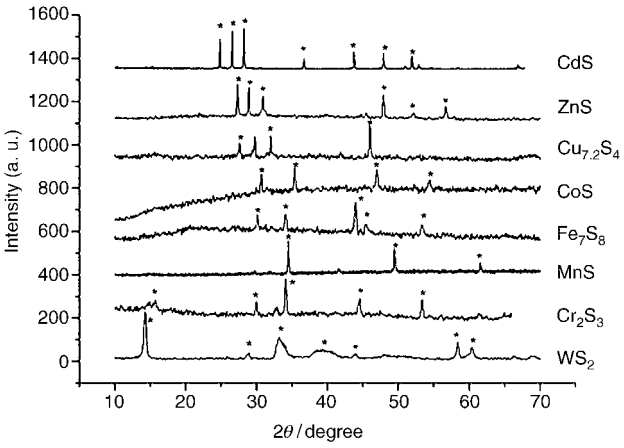

Figure 7. XRD patterns for the transition metal sulfide nanostructures.

The reaction to form these sulfides 1D nanostructures can be formulated as follows [Eq.(1)]:

$$MCl_x + S \rightarrow MS_y + S_2Cl_2$$
$$2\,S_2Cl_2 + 6\,NaOH \rightarrow 4\,NaCl + 3\,S + Na_2SO_3 + 3\,H_2O \quad (1)$$

Table 1. Summary of the as-prepared products. Structures were determined by XRD patterns.[a] The size and morphology were determined by using TEM images.[b]

Material	Structure	Morphology	Diameter [nm]	Length [μm]
CdS	H	NW	40–50	10
ZnS	H	NW	40–50	1–2
$Cu_{7.2}S_4$	FCC	NP	100	–
NiS	H	NW	40–50	10
CoS	H	NW	40–50	20–40
Fe_7S_8	H	NW	40–100	5–10
MnS	FCC	NW	40–100	10–20
Cr_2S_3	H	NR	100–150	1
WS_2	H	NT	20–30	5–10

[a] H = hexagonal and FCC = face-centered cubic. [b] NW = nanowire, NR = nanorod, NT = nanotube, NP = nanoparticle.

Chlorides (MCl_x) were chosen as the metal source, because they are proper precursors and have already been widely used to prepare many useful thin films.[25] They have a good thermal stability and do not decompose in the temperature regime used; they easily react at the desired temperature; and they often have a sufficiently high vapor pressure, which allows easy transported by the argon flow. Sulfur powder was selected as the S source, for it is less toxic than the H_2S gas, which is commonly used to prepare sulfide thin films. Large quantities of S powder created an atmosphere with excess sulfur to ensure that the MCl_x was completely changed into MS. The whole reaction system was strictly sealed and protected by the argon flow to avoid the formation of oxides at high temperature. Furthermore, a small quantity of the byproduct S_2Cl_2, a toxic material, is absorbed by a solution of NaOH (10 mol L^{-1}).

Growth mechanism: Further advancement of this synthetic route requires a clear understanding of the growth mechanism. However, real images of the growth process are always fuzzy and complicated, since these transition-metal sulfides all have their own unique properties. It's impossible to use one theory to explain the growth mechanism of all these 1D nanostructures, but regularities still could be concluded.

As mentioned in the Experimental Section below, single-crystal (100) Si wafers covered with a thin film of Au nanoparticles were used as substrate. The observation of nanospheres at the top of some nanowires, such as CdS, ZnS, and MnS, qualitatively suggests that the growth proceeds by a vapour–liquid–solid (VLS) mechanism (see Supporting Information Figure 1). This VLS crystal growth mechanism was originally proposed by Wagner and Ellis in 1964 for silicon whisker growth[26] and was recently re-examined by Lieber, Yang, and many other research groups to generate nanowires from a rich variety of inorganic materials. A typical VLS process starts with the dissolution of gaseous reactants into nanosized liquid droplets of a catalyst metal (such as Au here), followed by nucleation and growth of single-crystalline rods and then wires. For instance, in our system, hot vapor conating $CdCl_2$ and S species condenses into the Au-rich liquid nanocluster to form a pseudobinary liquid (Au–CdS). Nanowire growth begins after the liquid becomes supersaturated and continues as long as the Au–CdS remains in a liquid state and reactants $CdCl_2$ and S are available. Finally, it terminates when the furnace is cooled down and the Au–CdS nanocluster solidifies. It should be noted that the liquid droplet serves as a soft template to strictly limit the lateral growth of an individual wire, and its size should remain unchanged during the entire process of wire growth. In our experiment, the average diameter of the Au particles is 50 nm (see Supporting Information Figure 1), which is in agreement with the diameter of several nanowires. It strongly supports the VLS mechanism and also implies the diameter could be controlled by the size of Au particles pre-deposited.

As for the Cr_2S_3 nanorods, no small cluster was observed at the top; this indicates that the growth may be dominated by the vapour–solid (VS) mechanism. In this sense, $CrCl_3$ and S react to generate the initial nucleation, which grows in an epitaxial way and favors the formation of rods. In conclusion, the growth could be well explained by the VLS and VS mechanisms.

Crystallographic study of the sulfide 1D nanostructures: It is fairly hard to explain why these sulfides prefer to grow into 1D nanostructures, because the practical factors that have influence are more complex than we thought. However, the intrinsic crystallographic characters often dominate in the final morphology of the products in many instances; this should be paid more attention and study. Previous researchers have made some investigations and gave us abundant data for deep research. Duan and Lieber once reported a series of semiconductor nanowires fabricated by means of laser ablation.[19] Most of these wires, such as GaAs, GaP, InP, InAs, ZnS, and ZnSe, have the zinc blende structure and preferred to grow in (111) direction. They also mentioned two exceptions: CdS and CdSe. These wires have hexagonal structures and CdS prefers to grow in the (100) and (002) directions, while CdSe grows in the (110) direction. However, the intrinsic reason has not been revealed.

In this section, we made some fundamental investigations about the crystallographic characters and growth directions of hexagonal nanowires. From the nanostructures we synthesized, we choose CdS, CoS, NiS, and Fe_7S_8 nanowire for more intensive research. HRTEM images and electron diffraction patterns confirm that they grow along the (100),[27] (110),[28] (110) (Figure 2), and (003) (Supporting Information Figure 2) directions, respectively. As above, NiS will be the first subject investigated.

According to the Bravais' law, crystal faces with low index and large interplanar spacing are the first to form in the process of crystal growth. Based on our earlier observation (Figure 2c), we made a simple illustration (Figure 8) to describe the crystal face and growth direction of the wire. It is known that α-NiS has the hexagonal NiAs structure and has six equivalent crystal face directions (100, 010, −110 …) in the *xy* plane. Referring to the single-crystal data of the α-NiS, these low index surfaces have larger interplanar spacing ($d = 0.297826$ nm) than any other crystal faces. Therefore, the atoms prefer to stack in these directions, and the hexagonal nanowire might grow in (100) direction. However, the

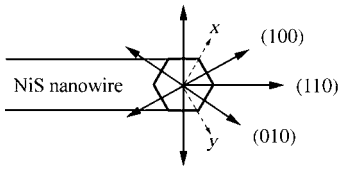

Figure 8. Crystallographic characteristics of the α-NiS nanowire. For details see text.

crystal growth may simultaneously occur in two preferred directions, such as (100) and (010), then the hexagonal nanowire would take the (110) direction as the wire axis. The HRTEM image in Figure 2c shows two crystal faces, which correspond to the (100) and (010) surfaces, that form an angle of 120° at the junction position; this confirms the rationality of our deductions. The same applies to the CoS nanowire, that is, it grows along the (110) direction owing to the simultaneous stack of the (100) and (010) crystal planes. Single-crystal data of these hexagonal sulfides from the JCPDS database may help the decision of the growth direction (Table 2).

Table 2. Single-crystal data of several hexagonal sulfides from the JCPDS database.

	CdS (No.77–2306)		CoS (No.75–0605)		NiS (No.77–1624)		Fe_7S_8 (No.76–2308)	
	hkl	*d*[Å]	*hkl*	*d*[Å]	*hkl*	*d*[Å]	*hkl*	*d*[Å]
1	100	3.58188	100	2.91851	100	2.97826	100	5.9461
2	002	3.35650	002	2.57000	002	2.66200	003	5.6960
3	101	3.16017	101	5.53793	101	2.59921	101	5.6158
$R=d_1/d_2$	1.067		1.136		1.119		1.044	

However, several instances still puzzle us: CdS and Fe_7S_8 nanowires should prefer to grow along the (100) or (110) directions according to the deduction above, whereas in reality they grow along (100), (002) and (003) directions. After attentive analysis, this phenomenon could be explained by the comparison of a specific parameter of each nanowire. Here, we define it as a special ratio $R=d_1/d_2$, in which d_1 and d_2 are the corresponding interplanar spacing of (100) and (00x) crystal face. Table 2 reveals that in most hexagonal structures the (00x) direction has the second largest interplanar spacing, only inferior to the (100) direction. According to the Bravais' law, the (00x) direction should also be a proper candidate. When the difference of the d value is not evident, the nanowire may also grow in the (00x) direction, such as CdS (100 or 002, $R=1.067$) and Fe_7S_8 (003, $R=1.044$). When the ratio of d_1 and d_2 is relatively large, the nanowire will certainly grow along the direction with larger interplanar spacing, such as CoS (110, $R=1.136$) and NiS (110, $R=1.119$).

In conclusion, nanowires with hexagonal structures prefer to grow along the (100), (110), or (00x) directions due to the particular interplanar spacing involved, and the d_1/d_2 value is quite significant to the final selection. Certainly, the conclusion is only a fundamental and qualitative understanding, but it may guide and predict the fabrication of other nanowires and crystal whiskers with hexagonal structures.

Conclusion

In summary, a series of transition-metal sulfide 1D nanostructures have been synthesized by means of a general APCVD strategy. VLS and VS mechanisms, along with the experimental results, were used to explain the formation of these 1D nanostructures. A regular conclusion about the growth direction of hexagonal nanowire has been drawn. Therefore, the adopted synthetic route is expected to provide many 1D building blocks for research into mesoscopic physics and fabrication of nanoscale devices.

Experimental Section

Materials: All reagents used in this work, including tungsten chloride (WCl_6), chromium chloride ($CrCl_3$), manganese chloride ($MnCl_2$), ferrous chloride ($FeCl_2$), cobalt chloride ($CoCl_2$), nickel chloride ($NiCl_2$), copper chloride ($CuCl_2$), zinc chloride ($ZnCl_2$), cadmium chloride ($CdCl_2$), and sulfur powder, were A. R. reagents (>99.99%) from the Beijing Chemical Factory (China) and were used directly. Single-crystal (100) Si wafers covered with a thin film of Au nanoparticles were cleaned prior to use by washing with ethanol, and subsequently dried in air.

Synthesis: Our growth apparatus was a furnace with a horizontal quartz tube; the temperature profile is shown in Figure 9. Various kinds of transition-metal chloride were placed in ceramic boat at the middle of the furnace, where the temperature could be exactly controlled. Sulfur powders (0.4 g) were put upstream, and the (100) Si wafer was located downstream. In an argon flow, the temperature was raised to a particular value with a heating rate 10 °C min^{-1} and remained at that point for 1–2 h. Then, the furnace was cooled down to room temperature slowly (~5 °C min^{-1}), and the products were deposited on the Si substrate. The specific parameters for the APCVD experiments are listed in Table 3.

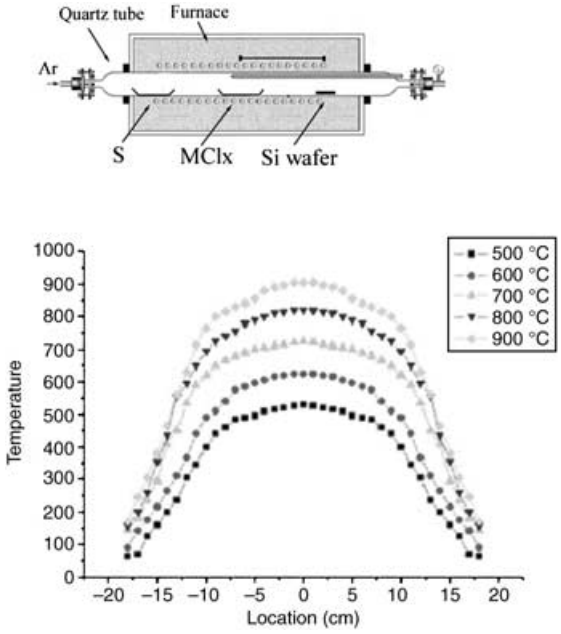

Figure 9. Apparatus and temperature profile of the furnace at different controlled temperature.

Table 3. The specific parameters for the APCVD of the transition-metal sulfides.

	Furnace T[°C]	Substrate T[°C][a]	Ar flow rate [sccm min^{-1}]	Run time [min]	XRD of product
$CdCl_2$	650	520	100	120	hexagonal CdS
$ZnCl_2$	750	480	100	120	hexagonal ZnS
$CuCl_2$	650	250	100	100	face-centered cubic $Cu_{7.2}S_4$
$NiCl_2$	700	620	100	120	hexagonal NiS
$CoCl_2$	850	580	100	100	hexagonal CoS
$FeCl_2$	900	600	100	120	hexagonal Fe_7S_8
$MnCl_2$	750	450	100	100	face-centered cubic MnS
$CrCl_3$	850	610	100	120	hexagonal Cr_2S_3
WCl_6	950	650	50	120	hexagonal WS_2

[a] The substrate temperature was estimated by comparing the wafer location with the temperature profile of the furnace.

Characterization: The samples was characterized by a Bruker D8 Avance X-ray diffractometer with $Cu_{K\alpha}$ radiation ($\lambda = 1.5418$ Å). The size and morphology of the as-prepared ZnS 1D nanostructures were obtained by using a Hitachi Model H-800 transmission electron microscope (with a tungsten filament at an accelerating voltage of 200 kV), a LEO 1530 scanning electron microscope, and a JEOL JEM-2010F high-resolution transmission electron microscope. EDAX was also measured by the TEM and HRTEM.

Acknowledgement

This work was supported by the NSFC (20025102, 50028201, 20151001), the Foundation for the Author of National Excellent Doctoral Dissertation of P. R. China, and the State Key Project of Fundamental Research for nanomaterials and nanostructures. Haiyan Dang and Dr. Liang Liu (Department of Physics, Tsinghua University) are thanked for the SEM observation.

[1] I. P. McClean, C. B. Thomas, *Semicond. Sci. Technol.* **1992**, *7*, 1394.
[2] L. Weinhardt, *Appl. Phys. Lett.* **2003**, *82*, 571.
[3] W. Chen, A. G. Joly, J. Z. Zhang, *Phys. Rev. B* **2001**, *64*, 041202.
[4] H. S. Yang, P. H. Holloway, B. B. Ratna, *J. Appl. Phys.* **2003**, *93*, 586.
[5] D. J. Norris, N. Yao, F. T. Charnock, T. A. Kennedy, *Nano Lett.* **2001**, *1*, 3.
[6] C. Chen, Z. Gao, W. Qin, *J. Appl. Phys.* **1991**, *70*, 6277.
[7] W. M. Kriven, *J. Am. Ceram. Soc.* **1988**, *71*, 1021.
[8] N. Keller, C. Phamhuu, C. Estournes, M. J. Ledoux, *Catal. Lett.* **1999**, *61*, 151.
[9] R. Cid, P. Atanasova, R. L. Cordero, J. M. Palacios, A. L. Agudo, *J. Catal.* **1999**, *182*, 328.
[10] J. Hu, T. W. Odom, C. M. Lieber, *Acc. Chem. Res.* **1999**, *32*, 435.
[11] Z. L. Wang, *Adv. Mater.* **2000**, *12*, 1295.
[12] M. H. Huang, S. Mao, H. Feick, H. Yan, Y. Wu, H. Kind, E. Weber, R. Russo, P. Yang, *Science* **2001**, *292*, 1897.
[13] X. G. Peng, L. Manna, W. D. Yang, *Nature* **2000**, *404*, 59.
[14] H. Q. Cao, Y. Xu, J. M. Hong, H. B. Liu, G. Yin, B. L. Li, C. Y. Tie, Z. Xu, *Adv. Mater.* **2001**, *13*, 1393.
[15] Y. D. Li, X. L. Li, R. R. He, J. Zhu, Z. X. Deng, *J. Am. Chem. Soc.* **2002**, *124*, 1411.
[16] Y. D. Li, H. W. Liao, Y. Ding, Y. Fan, Y. Zhang, Y. T. Qian, *Inorg. Chem.* **1999**, *38*, 1382.
[17] Y. D. Li, H. W. Liao, Y. Ding, Y. T. Qian, L. Yang, G. E. Zhou, *Chem. Mater.* **1998**, *10*, 2301.
[18] Y. Xie, L. Y. Zhu, X. C. Jiang, J. Lu, X. W. Zheng, W. He, Y. Z. Li, *Chem. Mater.* **2001**, *13*, 3927.
[19] X. F. Duan, C. M. Lieber, *Adv. Mater.* **2000**, *12*, 298.
[20] A. M. Morales, C. M. Lieber, *Science* **1998**, *279*, 208.
[21] Z. W. Pan, Z. R. Dai, Z. L. Wang, *Science* **2001**, *291*, 1947.
[22] Y. Jiang, X. M. Meng, J. Liu, Z. Y. Xie, C. S. Lee, S. T. Lee, *Adv. Mater.* **2003**, *15*, 323.
[23] Y. W. Wang, G. W. Meng, L. D. Zhang, C. H. Liang, J. Zhang, *Chem. Mater.* **2002**, *14*, 1773.
[24] S. Wang, S. Yang, *Chem. Mater.* **2001**, *13*, 4794.
[25] A. Harsta, *Chem. Vap. Deposition* **1999**, *5*, 191.
[26] R. S. Wagner, W. C. Ellis, *Appl. Phys. Lett.* **1964**, *4*, 89.
[27] H. P. Ge, Y. D. Li, *Adv. Funct. Mater.* **2004**, *14*, 157.
[28] J. P. Ge, Y. D. Li, *Chem. Commun.* **2003**, 2498.

Received: January 6, 2004
Published online: May 26, 2004

